ACS APPLIED MATERIALS & INTERFACES

Research Article

Cite This: ACS Appl. Mater. Interfaces 2019, 11, 13694−13703

www.acsami.org

Highly Robust MOF Polymeric Beads with a Controllable Size for Molecular Separations

Julien Cousin-Saint-Remi,*[,†] Stijn Van der Perre,[†] Tiriana Segato,[‖] Marie-Paule Delplancke,[‖] Steven Goderis,[‡] Herman Terryn,[§] Gino Baron,[†] and Joeri Denayer[†]

[†]Chemical Engineering Department, [‡]Analytical, Environmental and Geochemistry, and [§]Electrochemical and Surface Engineering Research Group, Vrije Universiteit Brussel, B-1050 Brussels, Belgium

[‖]Department of Materials Engineering, Characterization, Synthesis and Recycling, Université Libre de Bruxelles, B-1050 Bruxelles, Belgium

Supporting Information

ABSTRACT: Shaping metal−organic frameworks (MOFs) into robust particles with a controllable size is of large interest to the field of adsorption. Therefore, a method is presented here to produce robust MOF beads of different sizes, ranging from 250 μm to several millimeters, which, moreover, preserve the adsorption properties of the unformulated MOF. A simple, mild, and flexible method is demonstrated with the zeolitic imidazolate framework-8 (ZIF-8)/polyvinyl formal composite material. The properties of the composite material are determined via optical imaging, scanning electron microscopy, energy-dispersive X-ray spectroscopy, inductively coupled plasma mass spectrometry, X-ray diffraction, mercury intrusion, argon porosimetry and pycnometry as well as thermogravimetric analysis/differential scanning calorimetry, crush strength tests, and immersion experiments. The proposed method allows the production of resistant particles with a high MOF loading (up to 85 wt %) and remarkable structural and textural properties required for adsorptive separation processes, including a preserved ZIF-8 crystalline structure, microporosity, and a narrow macropore size distribution (1.27 μm average). The particles show a spherical shape with an average aspect ratio of 0.85. The stability tests demonstrated that the composite MOF material exhibits a high mechanical strength (3.09 N/Pc crushing strength) almost equivalent to that of a widely used commercial zeolite material. Furthermore, the material remains stable up to 200 °C and in most solvents. The adsorption properties are explored via static and dynamic experiments in the vapor and liquid phases. The results show that the adsorption capacities are only reduced in proportion to the binder content compared with the pristine material, indicating no binder intrusion in the ZIF-8 pores. Fixed-bed experiments demonstrate the remarkable separation performance in the vapor phase, whereas mass transfer limitations arise in the liquid phase with increasing flow rate. The mass transfer limitations are attributed to the diffusion in the macropores or through the ZIF-8 crystal outer layer.

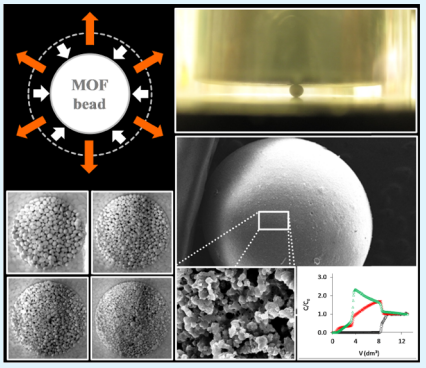

KEYWORDS: *metal-organic frameworks (MOFs), ZIF-8, shaping, powder processing, adsorption*

1. INTRODUCTION

Shaping porous materials into robust structures is a key aspect in the design of adsorption technologies.[1−5] In this perspective, metal−organic frameworks (MOFs) have been shaped into various structures, such as membranes,[6−9] foams,[10,11] and monoliths.[12−19] Recently, the formulation of MOFs (crystals) into resistant beads has also been gaining considerable attention.[20−29] Although structured adsorbents are seen as superior for mass and heat transfer or pressure drop issues,[4,5,30−32] most adsorptive separation processes are performed under fixed-bed conditions with adsorbent pellets as a result of their simplicity in column packing.[33] Therefore, the production of resistant MOF particles remains of large interest to the field of adsorption.

Various techniques, including extrusion, pressing, and granulation, can be used to process (unformulated) crystalline powder into beads.[30,34,35] Formulation methods for conventional materials, such as zeolites and active carbons, were developed decades ago and are routinely used in the large-scale production of commercial adsorbents and catalysts.[5,30,36−41] The organic linker of MOFs together with their limited stability imposes practical limits on the formulation method; for example, the high-temperature treatment under oxidative conditions typically applied with clay binders cannot be used.[35] Also, the pressing of (binder-free) MOF powders has been shown to lead to significant adsorption capacity losses.[42−44] Nevertheless, MOFs have been formulated with binder materials, including natural or synthetic polymers,[20−26] and different supports[27−29] and via various methods, such as phase inversion or granulation.[20−24] However, most studies display

Received: January 9, 2019
Accepted: March 21, 2019
Published: March 21, 2019

DOI: 10.1021/acsami.9b00521
ACS Appl. Mater. Interfaces 2019, 11, 13694−13703

losses in the adsorption capacity and mass transfer properties upon shaping, which may result from structural degradation or binder intrusion in the adsorbent pores,[10,16,17,19,21,23,45] but they also typically lack in exploring the material stability, particle size variation, or performance under dynamic conditions. Toward their implementation in adsorptive separation applications, the formulated MOF materials should possess high chemical, thermal, and mechanical stability, besides preserving or enhancing the remarkable adsorption properties of the unformulated MOF material. Finally, it is also important to develop formulation methods that are easily scalable to the large-scale production of the structured adsorbents.[23,29,33,34]

Therefore, in this study, a flexible method is proposed to produce resistant MOF beads of different particle sizes at the gram scale. To this end, we chose to work with the zeolitic imidazolate framework-8 (ZIF-8) as the MOF material.[46] It was previously identified as a promising adsorbent for the recovery and separation of biobutanol from acetone−butanol−ethanol (ABE) fermentation broths.[47,48] Besides its exceptional thermal and chemical stability compared with other MOF materials,[46,49] ZIF-8 is also one of the few MOFs that is currently commercially available in substantial quantities at an acceptable price, at least for research purposes. Furthermore, to generate a resistant structure that holds the ZIF-8 crystals together, we recently identified polyvinyl formal (PVFM) as an efficient binder to produce MOF/polymer hybrid particles.[50] Therefore, the ZIF-8/PVFM MOF polymeric composite material was selected as the ideal candidate to develop a flexible method for the formulation of MOFs at the gram scale and to investigate its effect on the adsorption properties and separation performance. Here, a complete study is performed starting from the production of composite MOF−polymeric particles up to the evaluation of their (separation) performance under dynamic conditions. A large set of characterization techniques was used to gain insight into the structural, textural, chemical, and adsorption properties of the formulated material as well as its mechanical, thermal, and chemical stability in the context of biobutanol recovery. In addition, mass transfer limitations are identified, and guidelines are provided for further optimization of the particles in accordance to (real) dynamic process conditions.

2. MATERIALS AND METHODS

2.2. ZIF-8 Materials and Characterization. ZIF-8 powder was purchased from Sigma-Aldrich (BASF Z1200, CAS 59061-53-9). Polymeric beads consisting of ZIF-8 crystals with polyvinyl formal (PVFM) binder (powder, CAS 9003-33-2, Sigma-Aldrich) were produced by an immersion precipitation method (see further). Chemical and structural properties of the ZIF-8 materials were characterized by optical images, scanning electron microscopy (SEM), energy-dispersive X-ray spectroscopy (EDX), mercury intrusion, argon porosimetry and pycnometry, and thermogravimetric analysis/differential scanning calorimetry (TGA−DSC). The mechanical and chemical resistance was determined by crush and immersion experiments, respectively. The adsorption properties (i.e., equilibria and kinetics) were measured, in the vapor and liquid phases, with a gravimetric method and batch measurements. The separation performance under dynamic conditions was evaluated with fixed-bed experiments. Details on the different techniques as well as the (supplier) properties of ZIF-8 and PVFM are provided in the Supporting Information.

2.3. Immersion Precipitation Method. An immersion precipitation method was developed to prepare MOF beads with a controllable particle size. General aspects on immersion precipitation, also called phase inversion, can be found elsewhere.[51−53] First, polyvinyl formal (PVFM) (0.882 g) was dissolved in dimethylformamide (DMF, 18 mL) (HPLC grade, Aldrich) at 353 K during 10 min. Once the polymer was dissolved, the ZIF-8 powder (5 g) was directly added and mixed to the hot polymer solution to create a viscous slurry. The relative dry mass of the PVFM binder (vs ZIF-8) was 15 wt % in most cases, but binder contents of 20 and 33 wt % were also explored. Afterward, while continuously stirring, the solvent (i.e., dimethylformamide, DMF; Sigma-Aldrich) was further evaporated from the slurry until the desired viscosity was attained to guarantee the efficient formation of beads. The required viscosity, being 1099 g/(m s), was determined by free-falling sphere experiments (Supporting Information). The slurry was then loaded into the piston of the setup (Figure 1).

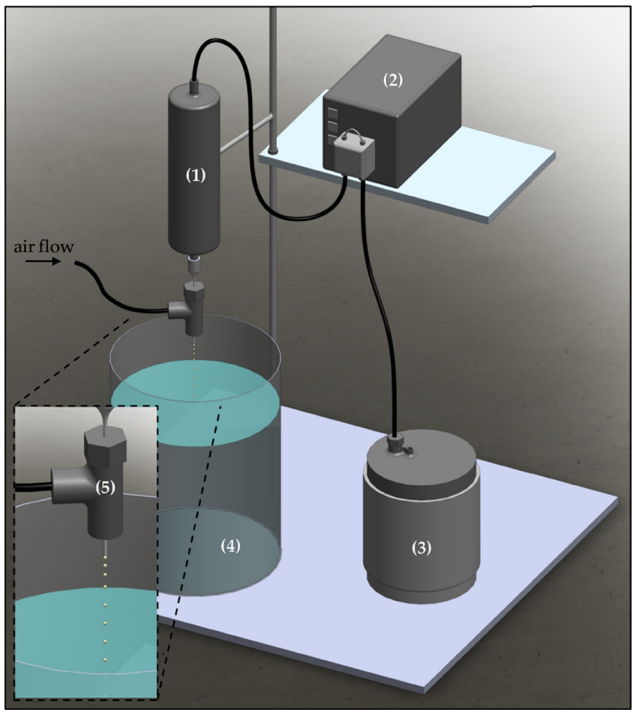

Figure 1. Immersion precipitation method, consisting of a piston (1), a pump (2), a pump fluid reservoir (3), a solvent reservoir (4), and a T-connecting piece (5).

The MOF beads were produced by the dropwise falling of the slurry, from the needle connected to the piston, into the liquid tank filled with distilled deionized water (SIMPAKOD2, Millipore) at 294 K. The piston was constructed out of two syringes: the bottom one loaded with the slurry and the upper one, which served to empty the bottom one, getting filled with the liquid at 1 mL/min, pumped from a separate reservoir. The piston was placed above the water tank such that the needle tip was set at 4 cm from the water surface. A needle with 0.9 mm inner diameter and a bevel tip (NN-2050R Neolus, Terumo) was used. In addition, a 1/8 in. Swagelok T-connecting piece, sealed with a septum at the upper side, was placed around the needle, allowing air to flow over the needle tip. The T-connecting piece was arranged in such a way that the needle protruded out by 3 mm. The increase in drag force due to the air flow enabled the reduction of the size at which the droplets were falling into the water tank and leading to the formation of smaller beads (see further). The air flow was varied between 0 and 3.2 L_N/min. Finally, once the piston was emptied from the slurry, the droplets, which hardened instantaneously on coming in contact with water, were separated from the liquid excess and dried overnight at 363 K. Considering that DMF is toxic, for safety reasons, the above-described method was performed under a fume hood.

DOI: 10.1021/acsami.9b00521
ACS Appl. Mater. Interfaces 2019, 11, 13694−13703

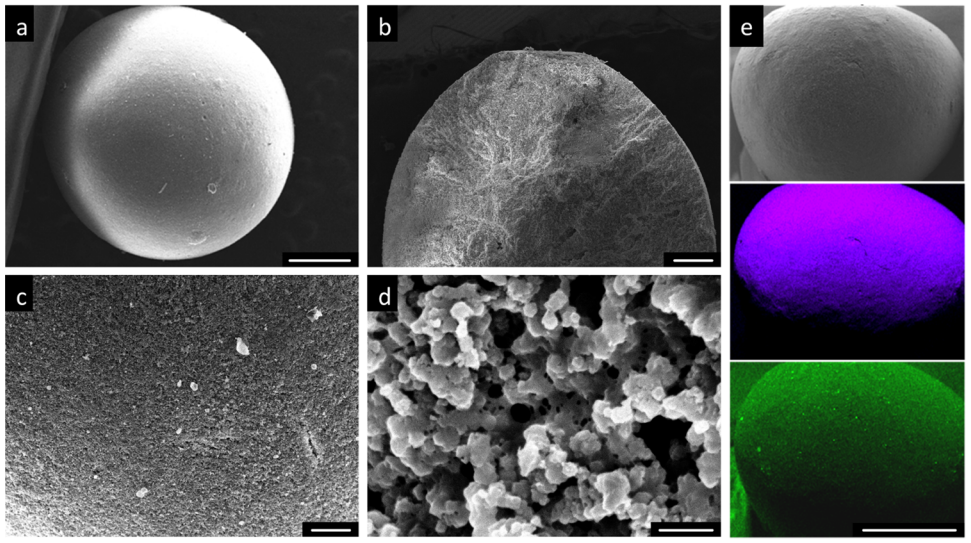

Figure 2. SEM−EDX images of ZIF-8/PVFM polymeric beads (with 15 wt % of PVFM): (a) shape, (b) inner (sectional) surface, (c,d) outer surface, and (e, middle) Zn mapping and (e, bottom) O mapping. Scale bars: (a) 500 μm, (b) 200 μm, (c) 50 μm, (d) 2 μm, and (e) 1 mm (see Supporting Information, Section S3, for more details).

Table 1. Textural Properties and Chemical Composition of ZIF-8, PVFM, and the Composite Material[a]

	EDX				ICP	He	Ar		Hg			
	Zn (atom %)	N (atom %)	C (atom %)	O (atom %)	Zn (wt %)	v_{He} (g/mL)	$v_{0.2,Ar}$[b] (mL/g)	$v_{0.8,Ar}$[b] (mL/g)	v_{Hg} (g/mL)	$v_{tot,Hg}$ (mL/g)	$v_{tot,Hg}$ (%)	$d_{p,avg}$ (μm)
ZIF-8[c]	9.8	26.7	63.6	0	29.5	1.487	0.448	0.649	0.503	0.83	52	0.29
PVFM	0	0	71.4[d]	28.6[d]		1.282	0.003	0.016				
composite	7.5	20.3	65.5	6.71	26.7	1.449	0.413	0.583	0.374	1.70	69	1.27

[a]With 15 wt % of PVFM. [b]Pore volume at p/p_{sat} = 0.2 and 0.8 (extracted from Figure 3). [c]EDX and Ar were carried out with powder, whereas binder-free (compacted) pellets were used for He and Hg. [d]According to the skeletal formula (see Table S1, Supporting Information).

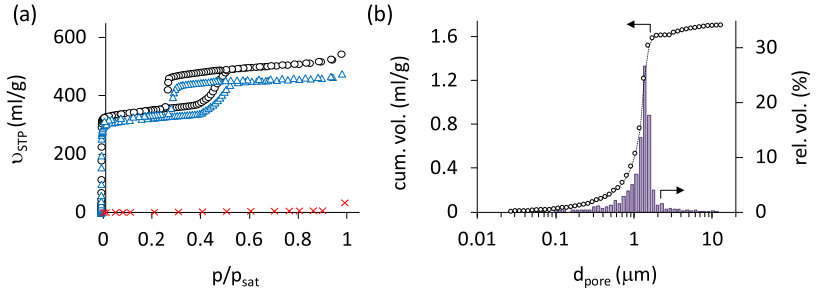

Figure 3. (a) Argon adsorption−desorption isotherm at 87 K on (○) ZIF-8 powder, (green triangle up solid) ZIF-8/PVFM composite material (with 15 wt % of PVFM), and (red times) PVFM. (b) Pore size distribution obtained from mercury intrusion experiments (more details in Supporting Information).

3. RESULTS AND DISCUSSION

3.1. Structural, Textural, and Chemical Properties of ZIF-8/PVFM Composite Beads. First, MOF/polymer composite beads (containing 15 wt % of the polymer) were produced without varying their size (i.e., no air flow used; see Materials and Methods; Figure 1). Properties of particles with different sizes (and also binder content) are discussed further in the manuscript. Figure 2 shows the textural properties and chemical mapping obtained by scanning electron microscopy (SEM) and electron-dispersive X-ray spectroscopy (EDX), respectively (see Supporting Information for more details), of ZIF-8/PVFM composite particles.

The characterization results indicate that the composite particles display a spherical shape, a diameter of about 2 mm (Figure 2a), and a well-defined smooth surface with limited debris and defects (Figure 2a,c). Sphericity deviations are limited as indicated by the SEM images (Figure 2b,e) and the average aspect ratio is 0.85 (see Supporting Information, Section S14). The PVFM polymer binder is seen to form a thin porous film holding the ZIF-8 crystals together (Figure 2d). In addition, the proposed method is found to disperse homogeneously the ZIF-8 crystals and the PVFM polymer binder on the surface (Figure 2c,d) and inside the particles (Figure 2b). This is also confirmed by the EDX mappings of zinc and oxygen, respectively (Figure 2e). Furthermore, the particles possess large pores, which are larger than the crystal size (Figure S1) and, moreover, uniformly distributed in the outer layer and inside the particles between the ZIF-8 crystals (Figure 2b,d). This feature is particularly important for fast mass transfer in the bulk of the beads.[33,54]

DOI: 10.1021/acsami.9b00521
ACS Appl. Mater. Interfaces 2019, 11, 13694−13703

Table 1 and Figure 3 provide additional characterization results obtained for the pure ZIF-8, the PVFM polymer binder, and the composite material. First, EDX analysis only detected oxygen in the PVFM polymer. Small oxygen sources known to be in the unformulated ZIF-8 powder, such as terminal hydroxyl groups, are not detected with this bulk method.[55−58] No difference in the Zn/N ratio is observed between the pure and the composite materials; however, Zn is detected in higher relative amounts than expected. On the other hand, via inductively coupled plasma mass spectrometry (ICP-MS), the zinc content was confirmed to be consistent with the ZIF-8 chemical formula (Table S2). Second, regarding the densities obtained by helium pycnometry (Table 1, He), also called skeletal densities, the density of (pure) ZIF-8 is consistent with those found in the literature.[59,60] The density of the composite material is lower than that of the pure ZIF-8 material due to the presence of the lighter compound (i.e., PVFM). Third, the argon adsorption−desorption isotherms (Figure 3a) demonstrate that the polymer barely takes up argon and that the isotherm shape is identical for ZIF-8 in both material states (i.e., unformulated and formulated). The latter indicates that the proposed formulation method preserves the argon adsorption properties of the pure (microporous) ZIF-8 MOF material. This is also supported by the X-ray diffraction (XRD) analysis, which demonstrates that the (bulk) structural properties are unaltered after the formulation of ZIF-8 (Figure S3). These remarkable results are attributed to the chemical stability of ZIF-8 in the formulation medium and the limited penetrability of PVFM inside the ZIF-8 pores. Figure 3a also points out that the composite material does not possess mesopores. Fourth, mercury intrusion reveals that the composite material is lighter than pure ZIF-8 (pellets), as seen from the pellet densities ρ_{Hg} (Table 1); however, the difference is much larger than for the skeletal densities (Table 1, ρ_{He}). This highlights the highly porous nature of the composite material, which is confirmed by the total (macro-)pore volumes $v_{tot,Hg}$ (Table 1). The pellet density is also found to be consistent with the calculated bulk density of the composite material, being 0.24 g/mL (see Supporting Information, Section S5). Furthermore, the average pore size $d_{p,avg}$ was found to be 1.27 μm (see also Figure 3b), which supports the SEM results (Figure 2d). In addition, our method appears to produce particles with a remarkably narrow pore size distribution (Figure 3b) with pores that were seen to be uniformly distributed within the particle (Figure 2b,d). Although the pore formation mechanism remains unclear,[61−63] it is speculated that the narrow pore distribution is formed because of the well-dissolved polymer being homogeneously distributed as a filamentous structure around the ZIF-8 crystals combined with an instant precipitation driven by the hydrophobic nature of both components in the composite material and the high affinity of DMF for water. The produced structure, combining microporous crystals interconnected by uniform and spatially well-distributed macropores, has been proposed as the preferred adsorbent structure for enhanced mass transfer during adsorptive separations.[64]

Furthermore, the amount of binder in the composite material was calculated from the different characterization results (Table 1). First, by comparing the argon porosities of both materials (i.e., pure ZIF-8 and composite particles) at 0.2 and 0.8 relative pressures (Table 1), corresponding to the low- and high-loading framework configurations of the (flexible) ZIF-8 MOF,[47,58,65−68] and assuming negligible argon uptake by the polymer (Figure 3a), the binder fraction is about 10 wt %. The same amount of binder is also estimated based on the ICP-MS results (Table 1). This is lower than that expected from the binder recipe (i.e., 15 wt %, see Materials and Methods). On the other hand, from the EDX analysis and helium pycnometry, the binder fraction corresponds to 17.4 and 16.15 wt %, respectively (see Supporting Information for more details), which are slightly higher but coherent with the binder recipe. Besides the limitations of each method (see Supporting Information), the sample size used in the various experiments may also explain these differences. Whereas the EDX analysis and helium pycnometry are performed on a large amount of particles (up to 2 g, see Supporting Information), argon porosimetry and ICP-MS are only performed on a few particles. This suggests that composite particles of one and the same batch may possess different binder contents, which most likely arise during the production of the MOF polymeric beads, where the slurry is no longer being mixed once loaded in the piston (Figure 1).

Finally, the results obtained with different probe molecules, namely helium, argon, and mercury, are connected with each other based on the different textural features enclosed in a pellet volume V_p.[69,70] It includes the volumes occupied by the material framework $V_{framework}$, the small pores $V_{small\ pores}$ (i.e., micro- and mesopores), and the larger (macro-)pores $V_{large\ pores}$. Since the composite material contains limited mesopores (Figure 3), the overlap between argon and mercury (intrusion) data is negligible, and the information obtained with the different probe molecules can be correlated by eq 1:

$$V_p = V_{framework} + V_{small\ pores} + V_{large\ pores} \approx V_{N/A,He} + V_{Ar} + V_{Hg} \quad (1)$$

with $V_{N/A,He}$, V_{Ar}, and V_{Hg} being the nonaccessible (helium) solid volume, the micro-/mesopore volume determined by argon porosimetry, and the volume of the macropores obtained by mercury intrusion, respectively. Equation 1 can be further written in relative amounts per mass adsorbent (in mL/g) from the densities and pore volumes as follows (eq 2):

$$\frac{1}{\rho_{Hg}} = \frac{1}{\rho_{He}} + v_{Ar} + v_{Hg} \quad (2)$$

Based on eq 2, it can be shown that the results displayed in Table 1 confirm one another, with differences between the left- and right-hand sides of eq 2 being only 4 or 10% depending on low-loading or high-loading ZIF-8 microporosities, respectively.

3.2. Mechanical, Thermal, and Chemical Stability. The mechanical, thermal, and chemical stabilities of the ZIF-8/PVFM composite material were evaluated by means of frictionless piston experiments, thermogravimetric analysis/differential scanning calorimetry (TGA−DSC), and immersion tests, respectively (see Supporting Information for more details). The results are summarized in Table 2.

Single-particle (crushing) tests reveal that the composite particles can support about 100 000 times their own weight before they break (Figure S4, left). As a packed bed, the particles can sustain a weight of at least 30.8 N (Table 2), which is the maximum measurable force with the current setup (see Supporting Information). Under such a mechanical stress, the pellets did not show any sign of degradation, but only a bed packing rearrangement was observed (Figure S4, middle and

DOI: 10.1021/acsami.9b00521
ACS Appl. Mater. Interfaces 2019, 11, 13694−13703

Table 2. Mechanical, Thermal, and Chemical Stability of the ZIF-8/PVFM Composite Material

crush strength (N)			
single particle	3.09 ± 0.97[a]		
bulk (packed bed)	>30.82[b,M]		
weight loss upon heating (wt %)			
	150 °C[c]	400 °C[c]	
ZIF-8	0.16	0.57	
PVFM	1.19	64.82	
composite	0.30	13.65	
stability upon immersion during 28 days			
ethanol	acetone	*n*BuOH	ABE
excellent	poor/excellent[c]	excellent	excellent

[a]± Standard deviation. [b]aximum measurable force was reached with the current setup. [c]btained from TGA–DSC curves (see Figure 4). [d]hen brought in contact with pure ethanol prior to being immersed in pure acetone.

right). On the other hand, commercially available adsorbents and catalysts possess bulk (crush) strength typically of at least 20 N (Table S3). A direct comparison was made with single-particle tests on commercial samples (Table S4). The results suggest that our method produces highly resistant adsorbent particles using a limited amount of polymer binder, which, moreover, almost reach the mechanical (crushing) stability of widely used commercial materials required for fixed-bed applications.

In addition, Table 2 provides the weight loss at two temperatures extracted from the TGA curves (determined under a flow of He) of ZIF-8, PVFM, and the ZIF-8/PVFM composite material (Figure 4a). First, no (significant) weight

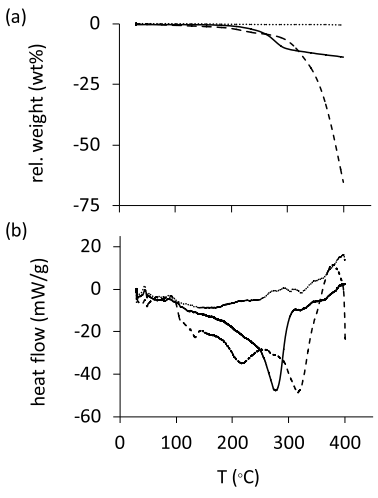

Figure 4. (a) TGA curves and (b) DSC curves of (dotted lines) the ZIF-8 powder, (dashed lines) PVFM, and (full lines) ZIF-8/PVFM composite particles (with 15 wt % of PVFM) under a helium flow (see Supporting Information, Section S7, for more details).

loss is observed for pure ZIF-8 MOF even at high temperature (see also Figure 4a). This is supported by former studies that indicate that ZIF-8 shows no structural degradation upon heating up to 823 K in an inert environment.[46,49] In contrast, although no significant weight loss is observed at low temperature, the pure PVFM polymer completely degrades at high temperature, also leading to a change in color, from white to black (not shown). These behaviors of both pure compounds are also observed with the composite material (Table 2). At low temperature (i.e., $\frac{c}{\lambda}$ 150 °C), the composite material remains stable, with unaltered adsorption properties as confirmed by cyclic adsorption–regeneration experiments (Figure S4), whereas at high temperature, it exhibits a weight loss corresponding to the amount of polymer (i.e., 15 wt %, see Methods) as well as a change in color, from white to gray (not shown). A thermal stability up to 150 °C could be regarded as sufficient considering the ease of regeneration/desorption from the ZIF-8 MOF material at low temperature.[47,48] Figure 4a indicates that the decomposition of the pure PVFM polymer starts at about 300 °C, with a continuous decrease in weight with increasing temperature. The composite material, however, shows a steep change in weight upon heating, corresponding most likely to the degradation of its polymer fraction. Interestingly, this decrease starts at a lower temperature than for the decomposition of the pure PVFM polymer. This is also corroborated by the DSC curves (Figure 4b), which exhibit two major (inversed) peaks for the pure PVFM polymer, whereas for the composite material only one peak is detected, at even a lower temperature. Such a shift has also been noticed for other MOF/polymer composite materials.[71,72] Furthermore, the different tendencies observed in Figure 4 are consistent with other studies that explored the TGA–DSC behaviors of pure PVFM and PVFM hybrid materials.[73−75] They correspond to the glass transition temperature, melting and crystallization, as well as the decomposition steps of PVFM.[73−75] A more detailed study is required to clearly distinguish these features and to understand the origin in the shift of the TGA–DSC curves of the composite material compared with those of the pure PVFM polymer.

Next, the chemical stability of the composite materials was assessed by immersion tests. ZIF-8/PVFM beads were immersed in liquid solutions containing compounds of the acetone–butanol–ethanol (ABE) fermentation.[47,48,76] Table 2 indicates that none of the pure liquids, except for acetone, damaged the macroscopic structure of the particles. Furthermore, pure PVFM was seen to be soluble in acetone, but not significantly in water or alcohols. Acetone will, therefore, most probably decompose the PVFM polymeric structure that holds the ZIF-8 crystals strongly together in the composite material. Interestingly, if ethanol is preadsorbed, the ZIF-8/PVFM composite particles retain their structure even after being contacted with acetone. This may be due to alcohol-induced polymer cross-linking, but the elucidation of this aspect lies beyond the scope of this work. The adsorption of alcohol molecules into the composite material may, thus, explain the excellent stability observed with the ABE mixture (Table 2). This protective effect is particularly interesting for adsorptive biobutanol recovery considering that ethanol elutes first from the column outlet during the ABE separation with ZIF-8 MOF-packed beds.[47,48] In other words, during this separation, the ethanol concentration front travels ahead of the acetone concentration front, and, thus, ethanol essentially saturates the particles inside the column prior to acetone. Besides maintaining its macroscopic structure, the composite material also remarkably preserves its adsorption properties after immersion tests (Figure S5). This is attributed to the chemical stability of the active (adsorptive) agent of the composite material, namely the ZIF-8 MOF.[46,49]

3.3. Adsorption Equilibria and Separation Performance. The adsorption properties (equilibria and kinetics) and, more

DOI: 10.1021/acsami.9b00521
ACS Appl. Mater. Interfaces 2019, 11, 13694−13703

importantly, the performance under dynamic conditions are the key information in the evaluation of an adsorbent material toward its implementation into a separation process.[33]

Figure 5 provides an overview of single-component adsorption (equilibrium) isotherms of ABE mixture compounds on the ZIF-8/PVFM composite material compared with those on the pure ZIF-8 MOF, obtained by a gravimetric method (see Supporting Information, Section S10). The adsorption isotherms of both materials possess the same shapes, with *n*-butanol having the largest affinity at low pressures (Figure 5a) compared with ethanol and acetone (Figure 5b,c) and water being almost completely excluded from the material pores (Figure 5d). It demonstrates that the affinity of the adsorbing compounds for the active agent of the composite material, namely the ZIF-8 crystals, is not affected by the formulation method, which is in line with the XRD and argon porosity analyses (vide supra). The capacities of the ZIF-8/PVFM composite material are, however, lower than those of the pure ZIF-8 MOF. Such a decrease in capacity is attributed to the PVFM polymeric binder.

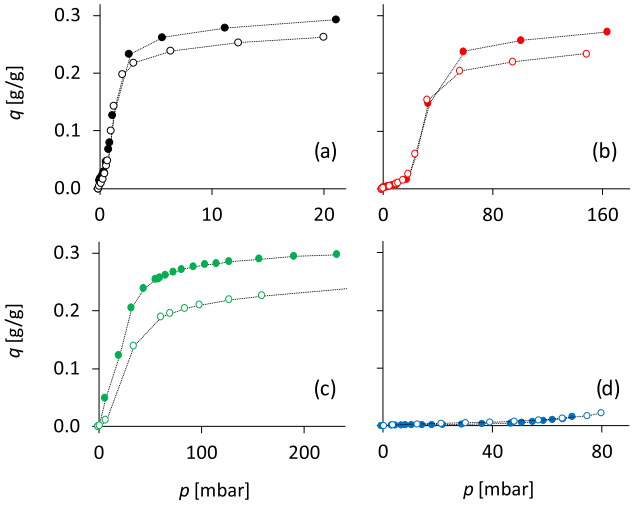

Figure 5. Vapor-phase adsorption isotherms of (a) *n*-butanol, (b) ethanol, (c) acetone, and (d) water on (filled symbols) the ZIF-8 powder[47] and (empty symbols) ZIF-8/PVFM composite particles (with 15 wt % of PVFM) at 323 K (more details in Supporting Information).

Furthermore, the dynamic separation performance was assessed by means of breakthrough experiments with packed beds (see Supporting Information). To this end, the feed flow rate was varied to identify mass transfer limitations that may occur during the separation of the ABE mixture with the ZIF-8/PVFM composite material. Furthermore, experiments were performed in both the vapor and liquid phases, toward two potential approaches to recover biobutanol from fermentation media.[47,48,77,78] The results are shown in Figure 6 for the liquid phase (Figure 6a,b) and the vapor phase (Figure 6c,d), at a low feed flow rate (Figure 6, top) and a high feed flow rate (Figure 6, bottom). In all cases, the three ABE compounds are well separated from each other, with ethanol eluting first from the packed column, followed by acetone, and *n*-butanol eluting last. This separation behavior is consistent with that of the pure ZIF-8 MOF material.[47,48] However, the elution curves, being composed of various overshoots and steps, exhibit different shapes for the liquid and vapor phases. Such shapes are the

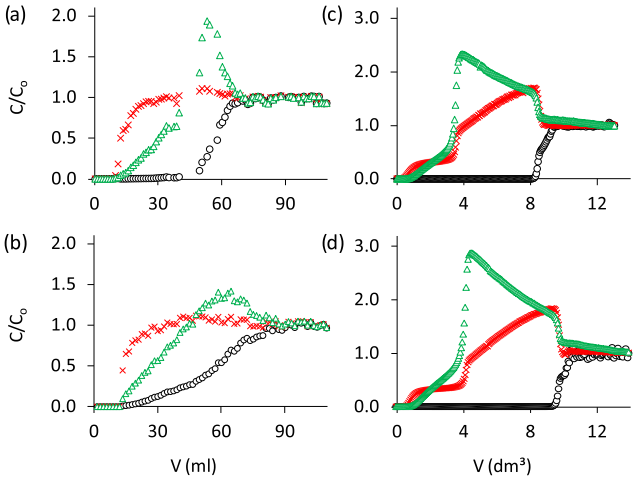

Figure 6. Breakthrough profiles of (red times) ethanol, (o) *n*-butanol, and (green triangle up solid) acetone in the presence of water on ZIF-8/PVFM composite particle-packed beds: (a, b) Liquid phase at 294 K and a flow rate of (a) 0.1 mL/min or (b) 0.3 mL/min; (c, d) Vapor phase at 323 K and a flow rate of (c) 10 mL/min or (d) 30 mL/min. Volumes are already corrected with the corresponding dead volume of the setup (see Supporting Information, Sections S9 and S10, for more details).

direct expression of the stepped or sigmoidal adsorption (equilibrium) isotherms and the different feed conditions.[33,47,79] Furthermore, whereas for the vapor phase the steepness of the elution profiles is unaffected by the feed flow rate (Figure 6c,d), under liquid conditions, the elution profiles at a high feed flow rate (Figure 6b) are much broader than those at a low feed flow rate (Figure 6a). This suggests that mass transfer limitations are more significant under liquid-phase conditions compared with those in the vapor phase. In other words, the large particles of the ZIF-8/PVFM composite material perform well in the vapor phase, whereas in the liquid phase the material should be optimized for a high feed flow rate, in particular, to reduce the mass transfer limitations leading to broad elution profiles.

3.4. Uptake Curves: Variation of Particle Size and Binder Content. To reduce mass transfer limitations, the overall (molecular) path length through the governing diffusion resistance(s) must be shortened.[33,54] Depending on their origin, this could be achieved, for example, by reducing the particle size or the binder layer thickness. In this section, these two parameters are varied to explore their effects on the molecular uptake rate by the ZIF-8/PVFM composite particles. For instance, smaller particles as well as particles with a higher binder fraction were prepared with the proposed method. The binder fraction was increased, because a decrease results in an unsuccessful particle production.

Figure 7a shows that this approach allows the production of particles from about 250 μm up to several millimeters. The average particle size is seen to be well controlled by varying the air flow rate, almost in a linear fashion; however, the variation is limited to a factor 2 in the investigated range (Figure 7b). The increase in the air (drag) flow rate decreases the particle size (Figure 7b), but also broadens the particle size distribution (Figure 8a–g). On the other hand, although some particles appear to be significantly deformed (Figure 8e,f), the sphericity deviation, given by the (average) aspect ratio (Figure 7b), remains constant and limited for the different batches. The broadening of the particles size distribution results in the

DOI: 10.1021/acsami.9b00521
ACS Appl. Mater. Interfaces 2019, 11, 13694–13703

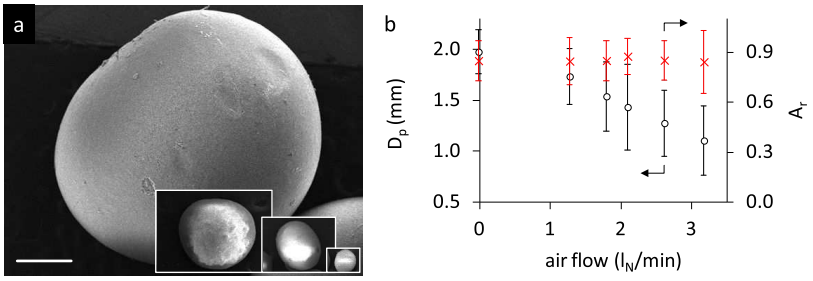

Figure 7. (a) SEM images of ZIF-8/PVFM particles (with 15 wt % of PVFM) of various sizes (scale bar: 500 μm) and (b) effect of the drag (air) flow rate on (○) the average particle size (volume based) and (red times) average aspect ratio with error bars (i.e., standard deviation, based on particle size distributions; see Supporting Information, Section 14)

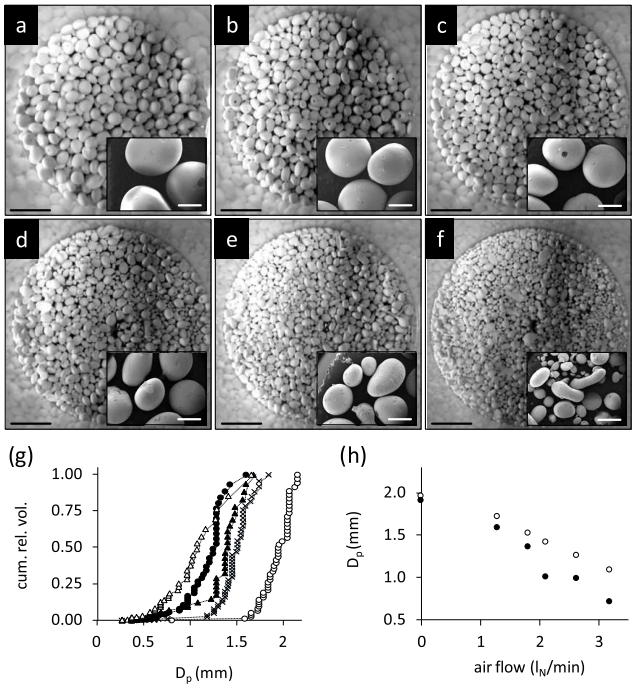

Figure 8. (a–f) Optical images (scale bar: 0.71 cm) of composite particles (with 15 wt % of PVFM) with zoom-in SEM images (scale bar: 1 mm). (g) Particle size distributions for batches obtained at different air flow rates: (○) 0, (−) 1.29, (×) 1.81, (▲) 2.11, (●) 2.63, and (Δ) 3.19 L_N/min. (h) Average particle sizes based on (filled symbols) frequency and (empty symbols) volume (see Supporting Information for more details).

divergence of the average particle size based on volume and frequency (Figure 8h).

Afterward, the different batches of ZIF-8/PVFM composite particles were tested with conventional (batch) uptake measurements in the vapor and liquid phases (see Supporting Information, Sections S8 and S11). A direct comparison between the uptake curves of the different batches was possible since the different ZIF-8/PVFM composite materials possessed the same adsorption equilibrium properties (i.e., identical or only reduced in proportion to the binder content; see Figure S5) and were made of ZIF-8 crystals from the same batch. Furthermore, even though it is well known that the identification of the governing diffusion resistance(s) with conventional (batch) techniques is very tedious and prone to large errors,[54,80] an attempt was made to provide a microscopic interpretation of the observed mass transfer limitations (vide supra) based on the uptake curves given in Figure 9.

In the vapor phase (Figure 9a,b), the molecular uptake by the formulated materials is systematically slower than that by the unformulated ZIF-8 MOF crystals. Interestingly, this decrease in the molecular uptake rate, induced by the formulation method, is not affected by the particle size (Figure 9a) or the binder content (Figure 9b). This suggests that the diffusion through the macropores or the polymeric binder layer is not the rate-limiting step under vapor-phase conditions. Bed diffusion can also be excluded considering the limited number of particles in the sample holder. Besides, heat effects also appear to be negligible since they would lead to a slower uptake for particles with a larger size and/or lower binder content compared with small particles with a high binder

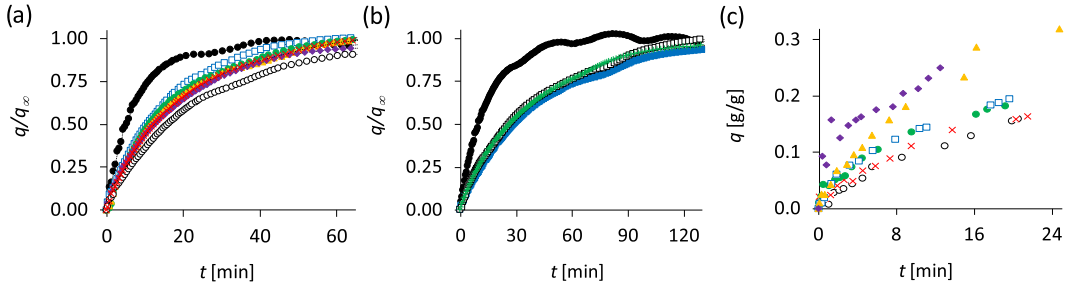

Figure 9. Uptake curves of *n*-butanol on ZIF-8 materials: (a) Vapor phase at 323 K and for a pressure step of 0.04–0.8 mbar, by (●) pure ZIF-8 MOF crystals and ZIF-8/PVFM composite particles (with 15 wt % of PVFM) with a (volume-based) average diameter of (○) 2.42, (red times) 2.28, (green circle solid) 1.96, (blue box) 1.54, (orange box) 1.27, or (purple box) 0.52 mm; (b) Vapor-phase uptake at 323 K and for a pressure step of 0–0.07 mbar, by (●) pure ZIF-8 MOF crystals and ZIF-8/PVFM composite particles with a (volume-based) average diameter of 1.97 mm and a binder content of (green plus) 15 wt %, (blue box) 20 wt %, and (□) 33 wt %; (c) Liquid-phase uptake at 294 K by ZIF-8/PVFM composite particles (with 15 wt % of PVFM) with a (volume-based) average diameter of (○) 1.97 mm, (red times) 1.72 mm, (●) 1.53, (blue box) 1.43 mm, (orange box) 1.27 mm, or (purple box) 1.10 mm.

DOI: 10.1021/acsami.9b00521
ACS Appl. Mater. Interfaces 2019, 11, 13694–13703

content. Therefore, we hypothesize that the mass transfer limitation arises from the blocking of the pore entrance by the PVFM polymer on the outer layer of ZIF-8 crystals. This will be investigated in future work, including approaches such as the further reduction of the binder content or preadsorption of the PVFM monomer on the ZIF-8 crystals (surface) prior to measuring the *n*-butanol uptake. On the other hand, the liquid-phase uptake of *n*-butanol by ZIF-8/PVFM composite particles (Figure 8c) is significantly affected by the particle size. The uptake times are, moreover, related to the square of the particle size. This proves that, under liquid-phase conditions, the mass transfer is limited by the diffusion in the macropores. Thus, depending on the (experimental) conditions, different mass transfer limitations govern the molecular uptake rate. Although the results of the batch uptake measurements (Figure 9) indicate that the use of smaller particles would be beneficial for a liquid-phase separation (Figure 6a,b), no such optimization seems to be required under dynamic vapor-phase conditions (Figure 6c,d). An assessment of the dynamic separation performance under (real) process conditions would, however, be needed toward the proper optimization of the ZIF-8/PVFM composite material.

4. CONCLUSIONS

In this work, an immersion precipitation method is presented, which allows the production of highly robust MOF particles with a controllable size from about 250 μm to several millimeters, and which preserves the specific adsorption properties of the unformulated MOF material. A simple, flexible, and mild method is demonstrated with the ZIF-8/PVFM MOF polymeric composite material. A complete study is performed starting from the production of the hybrid particles up to the evaluation of their separation performance. A large set of characterization techniques reveal that the formulation method produces highly resistant ZIF-8/PVFM particles with outstanding structural properties required for real adsorptive separation processes. On the other hand, static and dynamic adsorption experiments highlight that the adsorption equilibrium properties of the unformulated MOF are only reduced in proportion to the binder content. Also, depending on the process conditions, different mass transfer limitations govern the molecular uptake, such as diffusion resistance in the macropores or through the pore entrance of the ZIF-8 crystal outer layer. The specific optimization of the particle properties, however, should be performed in accordance with (real) dynamic process conditions. Furthermore, various aspects are highlighted from this work for further investigation, such as the origin of the mass transfer limitations, the stability improvement by preadsorption, or the thermal behavior of the polymer in the presence of MOF crystals. In addition, different modifications of our method will be explored to fine-tune the (total) porosity and (average) pore size in accordance to the process conditions. Finally, we believe that this method can be applied for the formulation of any MOF beads at a large scale and, consequently, to bring formulated MOF materials closer to commercialization and implementation in adsorption processes.

ASSOCIATED CONTENT

Supporting Information

The Supporting Information is available free of charge on the ACS Publications website at DOI: 10.1021/acsami.9b00521.

Additional material properties, free-falling sphere experiments, characterization methods, and dynamic and static adsorption experiments, EDX spectra, helium pycnometry, argon porosimetry and mercury intrusion, XRD patterns (PDF)

AUTHOR INFORMATION

Corresponding Author

*E-mail: jcousins@vub.be.

ORCID

Julien Cousin-Saint-Remi: 0000-0002-4937-1641

Herman Terryn: 0000-0003-2639-5496

Author Contributions

This manuscript was written through contributions of all authors. All authors have given approval to the final version of the manuscript.

Funding

The work was supported by the Research Foundation—Flanders (Belgium)

Notes

The authors declare no competing financial interest.

ACKNOWLEDGMENTS

J.C.-S.-R. and J.D. are grateful for the financial support of the Research Foundation—Flanders (12P2217N and 1512118N).

REFERENCES

(1) Stock, N.; Biswas, S. Synthesis of Metal-Organic Frameworks (MOFs): Routes to Various MOF Topologies, Morphologies, and Composites. *Chem. Rev.* **2012**, *112*, 933−969.

(2) Mueller, U.; Schubert, M.; Teich, F.; Puetter, H.; Schierle-Arndt, K.; Pastre, J. Metal−Organic Frameworks—Prospective Industrial Applications. *J. Mater. Chem.* **2006**, *16*, 626−636.

(3) Czaja, A. U.; Trukhan, N.; Müller, U. Industrial Applications of Metal−Organic Frameworks. *Chem. Soc. Rev.* **2009**, *38*, 1284−1293.

(4) Rezaei, F.; Webley, P. Optimum Structured Adsorbents for Gas Separation Processes. *Chem. Eng. Sci.* **2009**, *64*, 5182−5191.

(5) Borchardt, L.; Michels, N.-L.; Nowak, T.; Mitchell, S.; Pérez-Ramírez, J. Structuring Zeolite Bodies for Enhanced Heat-Transfer Properties. *Microporous Mesoporous Mater.* **2015**, *208*, 196−202.

(6) Qiu, S.; Xue, M.; Zhua, G. Metal−Organic Framework Membranes: from Synthesis to Separation Application. *Chem. Soc. Rev.* **2014**, *43*, 6116−6140.

(7) Hu, Y.; Dong, X.; Nan, J.; Jin, W.; Ren, X.; Xua, N.; Lee, Y. M. Metal−Organic Framework Membranes Fabricated via Reactive Seeding. *Chem. Commun.* **2011**, *47*, 737−739.

(8) Gascon, J.; Kapteijn, F. Metal-Organic Framework Membranes—High Potential, Bright Future? *Angew. Chem., Int. Ed.* **2010**, *49*, 1530−1532.

(9) Shah, M.; McCarthy, M. C.; Sachdeva, S.; Lee, A. K.; Jeong, H.-K. Current Status of Metal−Organic Framework Membranes for Gas Separations: Promises and Challenges. *Ind. Eng. Chem. Res.* **2012**, *51*, 2179−2199.

(10) Pinto, M. L.; Dias, S.; Pires, J. Composite MOF foams: the Example of UiO-66/Polyurethane. *ACS Appl. Mater. Interfaces* **2013**, *5*, 2360−2363.

(11) Chen, Y.; Huang, X.; Zhang, S.; Li, S.; Cao, S.; Pei, X.; Zhou, J.; Fen, X.; Wang, B. Shaping of Metal−Organic Frameworks: from Fluid to Shaped Bodies and Robust Foams. *J. Am. Chem. Soc.* **2016**, *138*, 10810−10813.

(12) Ahmed, A.; Forster, M.; Clowes, R.; Myers, P.; Zhang, H. Hierarchical Porous Metal−Organic Framework Monoliths. *Chem. Commun.* **2014**, *50*, 14314−14316.

DOI: 10.1021/acsami.9b00521
ACS Appl. Mater. Interfaces 2019, 11, 13694−13703

(13) Küsgens, P.; Zgaverdea, A.; Fritz, H.-G.; Siegle, S.; Kaskel, S. Metal-Organic Frameworks in Monolithic Structures. *J. Am. Ceram. Soc.* **2010**, *93*, 2476−2479.
(14) Ramos-Fernandez, E. V.; Garcia-Domingos, M.; Juan-Alcañiz, J.; Gascon, J.; Kapteijn, F. MOFs Meet Monoliths: Hierarchical Structuring Metal-Organic Framework Catalysts. *Appl. Catal., A* **2011**, *391*, 261−267.
(15) Thakkar, H.; Eastman, S.; Al-Naddag, Q.; Rownaghi, A. A.; Rezaei, F. 3D-Printed Metal-Organic Framework Monoliths for Gas Adsorption. *ACS Appl. Mater. Interfaces* **2017**, *9*, 35908−35916.
(16) Vilela, S. M.; Salcedo-Abraira, P.; Micheron, L.; Solla, E. L.; Yot, P. G.; Horcajada, P. A Robust Monolithic Metal-Organic Framework with Hierarchical Porosity. *Chem. Commun.* **2018**, *54*, 13088−13091.
(17) Hong, W. Y.; Perera, S. P.; Burrows, A. D. Manufacturing of Metal-Organic Framework Monoliths and their Application in CO_2 Adsorption. *Microporous Mesoporous Mater.* **2015**, *214*, 149−155.
(18) Lawson, S.; Rownaghi, A. A.; Rezaei, F. Carbon Hollow Fiber-Supported Metal-Organic Framework Composites for Gas Adsorption. *Energy Technol.* **2018**, *6*, 694−701.
(19) Rezaei, F.; Lawson, S.; Hosseini, H.; Thakkar, H.; Hajari, A.; Monjezi, S.; Rownaghi, A. A. MOF-74 and UTSA-16 Film Growth on Monolithic Structures and their CO2 Adsorption Performance. *Chem. Eng. J.* **2017**, *313*, 1346−1353.
(20) Li, L.; Yao, J.; Xiao, P.; Shang, J.; Feng, Y.; Webley, P. A.; Wang, H. One-Step Fabrication of ZIF-8/Polymer Composite Spheres by a Phase Inversion Method for Gas Adsorption. *Colloid Polym. Sci.* **2013**, *291*, 2711−2717.
(21) Abbasi, Z.; Shamsaei, E.; Fang, X.-Y.; Ladewig, B.; Wang, H. Simple Fabrication of Zeolitic Imidazolate Framework ZIF-8/Polymer Composite Beads by Phase Inversion Method for Efficient Oil Sorption. *J. Colloid Interface Sci.* **2017**, *493*, 150−161.
(22) Valekar, A. H.; Cho, K.-H.; Lee, U-H.; Lee, J. S.; Yoon, J. W.; Hwang, Y. K.; Lee, S. G.; Cho, S. J.; Chang, J.-S. Shaping of Porous Metal−Organic Framework Granules using Mesoporous ρ-Alumina as a Binder. *RSC Adv.* **2017**, *7*, 55767−55777.
(23) Ren, J.; Musyoka, N. M.; Langmi, H. W.; Swartbooi, A.; North, B. C.; Mathe, M. A More Efficient Way to Shape Metal-Organic Framework (MOF) Powder Materials for Hydrogen Storage Applications. *Int. J. Hydrogen Energy* **2015**, *40*, 4617−4622.
(24) Valizadeh, B.; Nguyen, T. N.; Smit, B.; Stylianou, K. C. Porous Metal−Organic Framework@Polymer Beads for Iodine Capture and Recovery Using a Gas-Sparged Column. *Adv. Funct. Mater.* **2018**, *28*, No. 1801596.
(25) Zheng, J.; Cui, X.; Yang, Q.; Ren, Q.; Yang, Y.; Xing, H. Shaping of Ultrahigh-Loading MOF Pellet with a Strongly Anti-tearing Binder for Gas separation and Storage. *Chem. Eng. J.* **2018**, *354*, 1075−1082.
(26) Avci-Camur, C.; Troyano, J.; Pérez-Carvajal, J.; Legrand, A.; Farrusseng, D.; Imaz, I.; Maspoch, D. Aqueous Production of Spherical Zr-MOF Beads via Continuous-Flow Spray-Drying. *Green Chem.* **2018**, *20*, 873−878.
(27) Aguado, S.; Caniveta, J.; Farrusseng, D. Facile Shaping of an Imidazolate-based MOF on Ceramic Beads for Adsorption and Catalytic Applications. *Chem. Commun.* **2010**, *46*, 7999−8001.
(28) O'Neill, L. D.; Zhang, H.; Bradshaw, D. Macro-/Microporous MOF Composite Beads. *J. Mater. Chem.* **2010**, *20*, 5720−5726.
(29) Yang, Q.; Zhao, Q.; Ren, S.; Chen, Z.; Zheng, H. Assembly of Zr-MOF Crystals onto Magnetic Beads as a Highly Adsorbent for Recycling Nitrophenol. *Chem. Eng. J.* **2017**, *323*, 74−83.
(30) Akhtar, F.; Andersson, L.; Ogunwumi, S.; Hedin, N.; Bergström, L. Structuring Adsorbents and Catalysts by Processing of Porous Powders. *J. Eur. Ceram. Soc* **2014**, *34*, 1643−1666.
(31) Rezaei, F.; Webley, P. Structured Adsorbents in Gas Separation Processes. *Sep. Purif. Technol.* **2010**, *70*, 243−256.
(32) Rezaei, F.; Grahn, M. Thermal Management of Structured Adsorbents in CO_2 Capture Processes. *Ind. Eng. Chem. Res.* **2012**, *51*, 4025−4034.
(33) Ruthven, D. *Principles of Adsorption and Adsorption Processes*; John Wiley: New York, 1984.
(34) Ren, J.; Langmi, H. W.; North, B. C.; Mathe, M. Review on Processing of Metal−Organic Framework (MOF) Materials Towards System Integration for Hydrogen Storage. *Int. J. Energy Res* **2015**, *39*, 607−620.
(35) Liu, Y.; Feng, Y.; Yao, J. Recent Advances in the Direct Fabrication of Millimeter-Sized Hierarchical Porous Materials. *RSC Adv.* **2016**, *6*, 80840−80846.
(36) Bingre, R.; Louis, B.; Nguyen, P. An Overview on Zeolite Shaping Technology and Solutions to Overcome Diffusion Limitations. *Catalysts* **2018**, *8*, 163.
(37) Giebelhausen, J.-M.; Spieker, H. Process for the Production of Shaped Activated Carbon. U.S. Patent US6316378B1, November 13, 2001.
(38) Burger, A.; Kaiser, H.; Ludovici, W. Production of Strong Active Carbon Moldings. U.S. Patent US3960761, June 1, 1976.
(39) Heinze, G.; Reiss, G.; Schwochow, F.; Ulisch, G. Zeolite Adsorbents. U.S. Patent US3773690, November 2, 1873.
(40) Heinze, G.; Podschus, E. Production of Silica Bonded Zeolitic Molecular Sieve Granules. U.S. Patent US3296151 A, January 3, 1967.
(41) Goytisolo, J. A.; Chi, D. D.; Lee, H. Process for Producing Zeolite X Molecular Sieve Bodies. U.S. Patent US3906076, September 16, 1975.
(42) Bazer-Bachi, D.; Assié, L.; Lecocq, V.; Harbuzaru, B.; Falk, V. Towards Industrial Use of Metal-Organic Framework: Impact of Shaping on the MOF Properties. *Powder Technol.* **2014**, *255*, 52−59.
(43) Peterson, G. W.; DeCoste, J. B.; Glower, T. G.; Huang, Y.; Jasuja, H.; Walton, K. S. Effects of Pelletization Pressure on the Physical and Chemical Properties of the Metal−Organic Frameworks Cu3(BTC)2 and UiO-66. *Microporous Mesoporous Mater.* **2013**, *179*, 48−53.
(44) Rezaei, F.; Sakwa-Novak, M. A.; Bali, S.; Duncanson, D. M.; Jones, C. W. Shaping Amine-based Solid CO2 Adsorbents: Effects of Pelletization Pressure on the Physical and Chemical Properties. *Microporous Mesoporous Mater.* **2015**, *204*, 34−42.
(45) Couck, S.; Cousin-Saint-Remi, J.; Van der Perre, S.; Baron, G. V.; Minas, C.; Ruch, P.; Denayer, J. F. M. 3D-printed SAPO-34 Monoliths for Gas Separation. *Microporous Mesoporous Mater.* **2018**, *255*, 185−191.
(46) Park, K. S.; Ni, Z.; Coté, A. P.; Choi, J. Y.; Huang, R.; Uribe-Romo, F. J.; Chae, H. K.; O'Keeffe, M.; Yaghi, O. M. Exceptional Chemical and Thermal Stability of Zeolitic Imidazolate Frameworks. *Proc. Natl. Acad. Sci. U.S.A.* **2006**, *103*, 10186−10191.
(47) Cousin Saint Remi, J.; Remy, T.; Van Hunskerken, V.; van de Perre, S.; Duerinck, T.; Maes, M.; De Vos, D.; Gobechiya, E.; Kirschhock, C. E. A.; Baron, G. V.; Denayer, J. F. M. Biobutanol Separation with the Metal−Organic Framework ZIF-8. *ChemSusChem* **2011**, *4*, 1074−1077.
(48) Cousin Saint Remi, J.; Baron, G.; Denayer, J. Adsorptive Separations for the Recovery and Purification of Biobutanol. *Adsorption* **2012**, *18*, 367−373.
(49) Yuan, S.; Feng, L.; Wang, K.; Pang, J.; Bosch, M.; Lollar, C.; Sun, Y.; Qin, J.; Yang, X.; Zhang, P.; Wang, Q.; Zou, L.; Zhang, Y.; Zhang, L.; Fang, Y.; Li, J.; Zhou, H.-C. Stable Metal−Organic Frameworks: Design, Synthesis, and Applications. *Adv. Mater.* **2018**, *30*, No. 1704303.
(50) Cousin-Saint-Remi, J.; Finoulst, A.-L.; Jabbour, C.; Baron, G. V.; Denayer, J. F. M. Selection of Binder Recipes for the Formulation of MOFs into Resistant Pellets for Molecular Separations by Fixed-Bed Adsorption. *Microporous Mesoporous Mater.* **2019**, DOI: 10.1016/j.micromeso.2019.02.009.
(51) Mulder, M. *Basic Principles of Membrane Technology*; Kluwer: Dordrecht, 1996.
(52) Binks, B. P. *Modern Aspects of Emulsion Science*; Royal Society of Chemistry: Cambridge, 1998.
(53) Hołda, A. K.; Vankelecom, I. F. J. Understanding and Guiding the Phase Inversion Process for Synthesis of Solvent Resistant Nanofiltration Membranes. *J. Appl. Polym. Sci.* **2015**, *132*, No. 42130.

DOI: 10.1021/acsami.9b00521
ACS Appl. Mater. Interfaces 2019, 11, 13694−13703

(54) Kärger, J.; Ruthven, D. M. *Diffusion in Zeolites and Other Microporous Solids*; John Wiley: New York, 1992.
(55) Karagiaridi, O.; Lalonde, M. B.; Bury, W.; Sarjeant, A. A.; Farha, O. K.; Hupp, J. T. Opening ZIF-8: a Catalytically Active Zeolitic Imidazolate Framework of Sodalite Topology with Unsubstituted linkers. *J. Am. Chem. Soc.* **2012**, *134*, 18790−18796.
(56) Zhang, K.; Lively, R. P.; Zhang, C.; Chance, R. R.; Koros, W. J.; Sholl, D. S.; Nair, S. Exploring the Framework Hydrophobicity and Flexibility of ZIF-8: from Biofuel Recovery to Hydrocarbon Separations. *J. Phys. Chem. Lett.* **2013**, *4*, 3618−3622.
(57) Canivet, J.; Vandichel, M.; Farrusseng, D. Origin of Highly Active Metal−Organic Framework Catalysts: Defects? Defects! *Dalton Trans.* **2016**, *45*, 4090−4099.
(58) Tanaka, S.; Fujita, K.; Miyake, Y.; Miyamoto, M.; Hasegawa, Y.; Makino, T.; Van der Perre, S.; Cousin Saint Remi, J.; Van Assche, T.; Baron, G. V.; Denayer, J. F. M. Adsorption and Diffusion Phenomena in Crystal Size Engineered ZIF-8 MOF. *J. Phys. Chem. C* **2015**, *119*, 28430−28439.
(59) Cao, S.; Bennett, T. D.; Keen, D. A.; Goodwind, A. L.; Cheetham, A. K. Amorphization of the Prototypical Zeolitic Imidazolate Framework ZIF-8 by Ball-Milling. *Chem. Commun.* **2012**, *48*, 7805−7807.
(60) Voskuilen, T. G.; Pourpoint, T. L.; Dailly, A. M. Hydrogen Adsorption on Microporous Materials at Ambient Temperatures and Pressures up to 50 MPa. *Adsorption* **2012**, *18*, 239−249.
(61) Li, W.-H.; Stöver, H. D. H. Porous Monodisperse Poly(divinylbenzene) Microspheres by Precipitation Polymerization. *J. Polym. Sci. Pol. Chem.* **1998**, *36*, 1543−1551.
(62) Smolders, C. A.; Reuvers, A. J.; Boom, R. M.; Wienk, I. M. Microstructures in Phase-Inversion Membranes. *J. Membr. Sci.* **1992**, *73*, 259−275.
(63) Gokmen, M. T.; Du Prez, F. E. Porous Polymer Particles − A Comprehensive Guide to Synthesis, Characterization, Functionalization and Applications. *Prog. Polym. Sci.* **2012**, *37*, 365−405.
(64) Ye, G.; Duan, X.; Zhu, K.; Zhou, X.; Coppens, M.-O.; Yuan, W. Optimizing Spatial Pore-Size and Porosity Distributions of Adsorbents for Enhanced Adsorption and Desorption Performance. *Chem. Eng. Sci.* **2015**, *132*, 108−117.
(65) Fairen-Jimenez, D.; Moggach, S. A.; Wharmby, M. T.; Wright, P. A.; Parsons, S.; Düren, T. Opening the Gate: Framework Flexibility in ZIF-8 Explored by Experiments and Simulations. *J. Am. Chem. Soc.* **2011**, *133*, 8900−8902.
(66) Moggach, S. A.; Bennett, T. D.; Cheetham, A. K. The Effect of Pressure on ZIF-8: Increasing Pore Size with Pressure and the Formation of a High-Pressure Phase at 1.47 GPa. *Angew. Chem., Int. Ed.* **2009**, *48*, 7087−7089.
(67) Fairen-Jimenez, D.; Galvelis, R.; Torrisi, A.; Gellan, A. D.; Wharmby, M. T.; Wright, P. A.; Mellot-Draznieks, C.; Duren, T. Flexibility and Swing Effect on the Adsorption of Energy-Related Gases on ZIF-8: Combined Experimental and Simulation Study. *Dalton Trans.* **2012**, *41*, 10752−10762.
(68) Tanaka, H.; Ohsaki, S.; Hiraide, S.; Yamamoto, D.; Watanabe, S.; Miyahara, M. T. Adsorption-Induced Structural Transition of ZIF-8: a Combined Experimental and Simulation Study. *J. Phys. Chem. C* **2014**, *118*, 8445−8454.
(69) Lowell, D. S.; Shields, J. E.; Thomas, M. A.; Thommes, M. *Characterization of Porous Solids and Powders: Surface Area, Pore Size and Density*; Kluwer: Dordrecht, 2004.
(70) Thommes, M. Physical Adsorption Characterization of Nanoporous Materials. *Chem. Ing. Tech.* **2010**, *82*, 1059−1073.
(71) Cacho-Bailo, F.; Seoane, B.; Téllez, C.; Coronas, J. ZIF-8 Continuous Membrane on Porous Polysulfone for Hydrogen Separation. *J. Membr. Sci.* **2014**, *464*, 119−126.
(72) Zornoza, B.; Seoane, B.; Zamaro, J. M.; Téllez, C.; Coronas, J. Combination of MOFs and Zeolites for Mixed-Matrix Membranes. *ChemPhysChem* **2011**, *12*, 2781−2785.
(73) Chetri, P.; Dass, N. N. Preparation of Poly (Vinyl Formal) of High Acetalization. *Polymer* **1997**, *38*, 3951−3956.
(74) Lian, F.; Guan, H.; Wen, Y.; Pan, X.-R. Polyvinyl Formal Based Single-Ion Conductor Membranes as Polymer Electrolytes for Lithium Ion Batteries. *J. Membr. Sci.* **2014**, *469*, 67−72.
(75) Guan, H.-Y.; Lian, F.; Xi, K.; Ren, Y.; Sun, J.-L.; Kumar, R. V. Polyvinyl Formal Based Gel Polymer Electrolyte Prepared using Initiator Free In-Situ Thermal Polymerization Method. *J. Power Sources* **2014**, *245*, 95−100.
(76) Lee, S. Y.; Park, J. H.; Jang, S. H.; Nielsen, L. K.; Kim, J.; Jung, K. S. Fermentative Butanol Production by Clostridia. *Biotechnol. Bioeng* **2008**, *101*, 209−228.
(77) Van der Perre, S.; Gelin, P.; Claessens, B.; Martin-Calvo, A.; Cousin Saint Remi, J.; Duerinck, T.; Baron, G. V.; Palomino, M.; Sánchez, L. Y.; Valencia, S.; Shang, J.; Singh, R.; Webley, P. A.; Rey, F.; Denayer, J. F. M. Intensified Biobutanol Recovery by using Zeolites with Complementary Selectivity. *ChemSusChem* **2017**, *10*, 2968−2977.
(78) Abdehagh, N.; Dai, B.; Thibault, J.; Tezel, F. H. Biobutanol Separation from ABE Model Solutions and Fermentation Broths using a Combined Adsorption−Gas Stripping Process. *J. Chem. Technol. Biotechnol.* **2017**, *92*, 245−251.
(79) Cousin-Saint-Remi, J.; Denayer, J. F. M. Applying the Wave Theory to Fixed-Bed Dynamics of Metal-Organic Frameworks Exhibiting Stepped Adsorption Isotherms: Water/ethanol Separation on ZIF-8. *Chem. Eng. J.* **2017**, *324*, 313−323.
(80) Cousin Saint Remi, J.; Lauerer, A.; Chmelik, C.; Vandendael, I.; Terryn, H.; Baron, G. V.; Denayer, J. F. M.; Kärger, J. The Role of Crystal Diversity in Understanding Mass Transfer in Nanoporous Materials. *Nat. Mater.* **2016**, *15*, 401−406.

DOI: 10.1021/acsami.9b00521
ACS Appl. Mater. Interfaces 2019, 11, 13694−13703